Journal of Electromagnetic Analysis and Applications, 2026, 18(6), 97-111
https://www.scirp.org/journal/jemaa
ISSN Online: 1942-0749
ISSN Print: 1942-0730

New Modeling of Horn Array Antenna Radiating in Free Space with Generalized Method-Floquet Modal Analysis

Abdessalem Kaddouri, Taoufik Aguili

Syscom Laboratory, National Engineering School of Tunis, Tunis El Manar University, le Belvédère, Tunisia
Email: abdessalem.kaddouri@enit.utm.tn, taoufik.aguili@enit.rnu.tn

How to cite this paper: Kaddouri, A. and Aguili, T. (2026) New Modeling of Horn Array Antenna Radiating in Free Space with Generalized Method-Floquet Modal Analysis. *Journal of Electromagnetic Analysis and Applications*, **18**, 97-111.
https://doi.org/10.4236/jemaa.2026.186006

Received: January 21, 2026
Accepted: June 27, 2026
Published: June 30, 2026

Abstract

This paper presents a novel and rigorous formulation for the analysis and optimization of horn antenna arrays radiating into free space. The proposed approach employs a two-stage global method. First, a single pyramidal horn antenna is modeled by combining the Method of Moments (MoM) with the Generalized Equivalent Circuit (GEC) method. The horn is decomposed as a cascade of rectangular waveguide discontinuities with gradually increasing transverse dimensions. This model enables a detailed parametric study of the horn's profile geometry and its influence on key radiation characteristics, including directivity and gain. In the second stage, Floquet modal analysis is applied to synthesize a periodic array from the optimized horn element. This allows for an efficient investigation of mutual coupling and the impact of inter-element spacing on the near-electric-field distribution across the array aperture. The numerical results obtained with the proposed method are presented and discussed, demonstrating good agreement with fundamental expectations and verifying the enforcement of electromagnetic boundary conditions. The formulation provides a computationally efficient and accurate tool for the design of high-performance horn arrays.

Keywords

Method of Moments (MoM), Generalized Equivalent Circuit (GEC), Floquet Analysis, Horn Antenna, Antenna Array, Mutual Coupling, Scattering Matrix, Waveguide Discontinuity

1. Introduction

The increasing demand for high-gain, low-sidelobe radiation patterns in modern wireless telecommunication, radar, and satellite systems has driven significant research into advanced antenna array configurations. Among these, waveguide-based arrays have been widely adopted due to their high power handling capacity, low loss, and mechanical robustness [1] [2]. In previous work [3]-[5], we developed a rigorous approach combining the Method of Moments (MoM) with the Generalized Equivalent Circuit (GEC) method to model finite rectangular waveguide arrays, incorporating Floquet modal analysis to efficiently handle periodic structures [6]. This method provided an accurate framework for analyzing mutual coupling, edge effects, and radiation pattern synthesis while mitigating the computational burden associated with large arrays.

Although rectangular waveguide arrays offer satisfactory performance in many applications, their direct radiation characteristics—such as limited bandwidth and moderate gain—can be further enhanced by employing horn elements. Pyramidal horns, in particular, are known for their improved directivity, lower reflection coefficients, and better impedance matching over broader frequency bands [7] [8]. However, the modeling of horn antennas—especially when arranged in arrays—introduces additional complexity due to their flared geometry and the electromagnetic interactions between adjacent elements. Traditional full-wave simulations of horn arrays become computationally prohibitive as the number of elements increases, necessitating the development of efficient yet accurate modeling techniques.

In this paper, we extend our earlier formulation to address the analysis and design of pyramidal horn arrays radiating into free space. The proposed approach is structured in two complementary stages. First, a single pyramidal horn is rigorously modeled using the MoM-GEC method, representing the horn as a cascade of rectangular waveguide sections with gradually expanding apertures. This allows for a detailed study of the impact of the horn profile—including flare angle and length—on key radiation characteristics such as directivity, gain, and sidelobe levels. Through parametric analysis, an optimized horn geometry is identified, balancing performance with physical dimensions.

In the second stage, the optimized horn element is integrated into a periodic array configuration. By employing Floquet modal analysis, we efficiently synthesize the array environment and examine the effects of inter-element spacing on the near-field distribution and mutual coupling between horns. This step enables the characterization of array-specific phenomena, including grating lobes and coupling-induced pattern distortions, which are critical for achieving desired far-field radiation patterns.

The proposed hybrid methodology not only preserves the rigor of full-wave analysis but also significantly reduces computational cost compared to direct simulation of the entire array. It thus provides a powerful tool for the design of high-performance horn arrays tailored to modern communication and radar applications.

The paper is organized as follows: Section II describes the MoM-GEC modeling of a single pyramidal horn. Section III details the extension to periodic arrays using Floquet modal analysis. Section IV presents numerical results and discussions, including validation against reference methods. Finally, Section V concludes the paper and suggests perspectives for future work.

2. Horn Waveguide

2.1. Study Structure

Our concept to model the horn waveguide is to juxtapose in the propagation axis "**z**" many concentric discontinuities with a same ratio, of a rectangular waveguide, toward a more appropriate dimension for radiation in the free space. Arriving to this dimension, we apply the discontinuity that opens into the free space.

2.2. Problem Formulation

We propose a formulation of a horn waveguide radiating in the free space divided into five parts (Figure 1), then we formulate the whole. The subdivisions are as follows

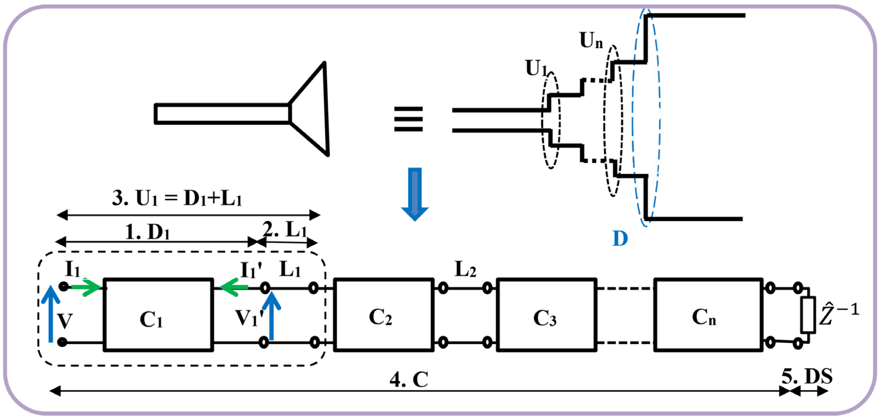

Figure 1. General view of the formulation of horn waveguide radiating in the free space.

1) The basic concentric discontinuity ***D***.
2) The line between two successive discontinuities ***L***.
3) The basic unit ***U***.
4) The chain of discontinuities until the aperture into space ***C***.
5) The discontinuity of the free space ***DS***.
6) The whole formulation.

2.2.1. Modeling of the Basic Concentric Discontinuity *D*

The study of the basic discontinuity D is similar to [1], except that this time the discontinuity plan does not separate an excited guide and another representing the load of the free space; but separate two excited guides G_1 and G_2. So we have two power supplies, each with its internal admittance. Figure 2(a) showing the structure of the discontinuity and Figure 2(b), its equivalent circuit.

In this figure, the two excitations are brought back to the discontinuity plane as modal current sources. The value of each is the current density of the fundamental mode $I_i f_i$, and its internal admittance is $\hat{Y}_i$. This latter represents the contribution of the evanescent modes of the waveguide G_i, and formal writing is:

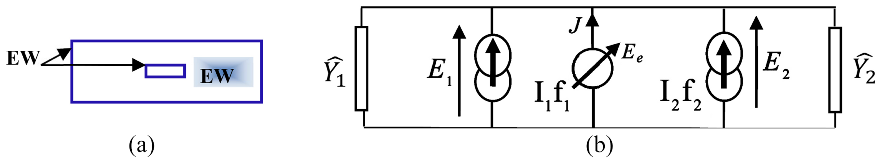

Figure 2. (a) Discontinuity structure, (b) the relative equivalent circuit.

$$\hat{Y}_i = \sum \left| F_{mn}^{(i)} \right\rangle y_{mn}^{(i)} \left\langle F_{mn}^{(i)} \right| \tag{1}$$

In this expression $F_{mn}^{(i)}$ form the modal basis of waveguide G_i except the fundamental mode F_i; and $y_{mn}^{(i)}$ is the admittance of each mode $F_{mn}^{(i)}$ [3].

The voltage across the terminals of the modal source $I_i f_i$ is E_i, is none other than its dual.

E_e is the virtual voltage source defined in the discontinuity plane, and J is the current flowing through it. Indeed, E_e is the unknown problem and is expressed as a series of test functions weighted by unknown modal amplitudes:

$$E_e = \sum_p x_p g_p \tag{2}$$

By applying the generalized Kirchhoff in Figure 2(b), we have the following equations:

$$E_e = E_1 = E_2 \tag{3}$$

$$J = -I_1 f_1 - I_2 f_2 + \left(\hat{Y}_1 + \hat{Y}_2\right) E_e \tag{4}$$

This can be written in matrix form as:

$$\begin{pmatrix} E_1 \\ E_2 \\ J \end{pmatrix} = \begin{pmatrix} 0 & 0 & 1 \\ 0 & 0 & 1 \\ -1 & -1 & \hat{Y}_1 + \hat{Y}_2 \end{pmatrix} \begin{pmatrix} I_1 f_1 \\ I_2 f_2 \\ E_e \end{pmatrix} \tag{5}$$

In aperture the current density is null, so Equation (4) is written:

$$0 = -I_1 f_0^{(1)} - I_2 f_0^{(2)} + \left(\hat{Y}_1 + \hat{Y}_2\right) E_e \tag{6}$$

Applying the Galerkin method, and taking into account the relation (2), we can reduce to the following system of equations:

$$\begin{cases} V_1 = \langle f_1 | E_1 \rangle = \sum_q x_q \langle f_1 | g_q \rangle = A_1^t X & (7) \\ V_2 = \langle f_2 | E_2 \rangle = \sum_q x_q \langle f_2 | g_q \rangle = A_2^t X & (8) \\ -I_1 \langle g_p | f_1 \rangle - I_2 \langle g_p | f_2 \rangle + \sum_q \left\langle g_p \middle| \left(\hat{Y}_1 + \hat{Y}_2\right) g_q \right\rangle x_q = 0 & (9) \end{cases}$$

The matrix writing of this system is:

$$\begin{pmatrix} V_1 \\ V_2 \\ 0 \end{pmatrix} = \begin{pmatrix} 0 & 0 & \langle f_1 | g_e \rangle \\ 0 & 0 & \langle f_2 | g_e \rangle \\ -\langle g_p | f_1 \rangle & -\langle g_p | f_2 \rangle & \left\langle g_p \middle| \left(\hat{Y}_1 + \hat{Y}_2\right) g_q \right\rangle \end{pmatrix} \begin{pmatrix} I_1 \\ I_2 \\ X \end{pmatrix} \tag{10}$$

If we consider that $A_1 = \left\langle g_p \middle| f_1 \right\rangle$, $A_2 = \left\langle g_p \middle| f_2 \right\rangle$ and $M = \left\langle g_p \middle| \left(\hat{Y}_1 + \hat{Y}_2\right) g_q \right\rangle$, we can write (10) as follow:

$$\begin{pmatrix} V_1 \\ V_2 \\ [0] \end{pmatrix} = \begin{pmatrix} 0 & 0 & A_1^t \\ 0 & 0 & A_2^t \\ -A_1 & -A_2 & M \end{pmatrix} \begin{pmatrix} I_1 \\ I_2 \\ X \end{pmatrix} \tag{11}$$

From the last line of this matrix, we can deduce the unknown from the problem:

$$X = M^{-1}\left(I_1 A_1 + I_2 A_2\right) \tag{12}$$

And we inject it into the first two lines, to obtain the following system of equations:

$$\begin{cases} V_1 = A_1^t M^{-1}\left(I_1 A_1 + I_2 A_2\right) & (13) \\ V_2 = A_2^t M^{-1}\left(I_1 A_1 + I_2 A_2\right) & (14) \end{cases}$$

We rewrite this system in a matrix form:

$$\begin{pmatrix} V_1 \\ V_2 \end{pmatrix} = \begin{pmatrix} A_1^t M^{-1} A_1 & A_1^t M^{-1} A_2 \\ A_2^t M^{-1} A_1 & A_2^t M^{-1} A_2 \end{pmatrix} \begin{pmatrix} I_1 \\ I_2 \end{pmatrix} \tag{15}$$

To deduce directly the Z matrix:

$$Z = \begin{pmatrix} A_1^t M^{-1} A_1 & A_1^t M^{-1} A_2 \\ A_2^t M^{-1} A_1 & A_2^t M^{-1} A_2 \end{pmatrix} \tag{16}$$

With the Z_{ij} terms which have the following generic form:

$$Z_{ij} = A_i^t M^{-1} A_j \tag{17}$$

We take (15) in the form of a system of equations:

$$\begin{cases} V_1 = Z_{11} \cdot I_1 + Z_{12} \cdot I_2 & (18) \\ V_2 = Z_{21} \cdot I_1 + Z_{22} \cdot I_2 & (19) \end{cases}$$

and extracts the expression of I_1 from (19):

$$I_1 = \left(V_2 - Z_{22} I_2\right) \cdot Z_{21}^{-1} \tag{20}$$

to inject it in (18):

$$V_1 = Z_{11} \cdot \left(V_2 - Z_{22} I_2\right) \cdot Z_{21}^{-1} + Z_{12} \cdot I_2 \tag{21}$$

Hence the following equations system:

$$\begin{cases} V_1 = Z_{11} Z_{21}^{-1} \cdot V_2 + \left(Z_{12} - Z_{11} Z_{22} Z_{21}^{-1}\right) \cdot I_2 & (22) \\ I_1 = Z_{21}^{-1} \cdot V_2 - Z_{22} Z_{21}^{-1} \cdot I_2 & (23) \end{cases}$$

which gives the passage matrix of the physical quantities relative to the port N˚1 to those relating to the port N˚2:

$$\begin{pmatrix} V_1 \\ I_1 \end{pmatrix} = \begin{pmatrix} Z_{11} Z_{21}^{-1} & Z_{12} - Z_{11} Z_{22} Z_{21}^{-1} \\ Z_{21}^{-1} & -Z_{22} Z_{21}^{-1} \end{pmatrix} \begin{pmatrix} V_2 \\ I_2 \end{pmatrix} \tag{24}$$

This matrix is none other than the chain matrix C_D which represents the discontinuity D:

$$C_D = \begin{pmatrix} Z_{11}Z_{21}^{-1} & Z_{12} - Z_{11}Z_{22}Z_{21}^{-1} \\ Z_{21}^{-1} & -Z_{22}Z_{21}^{-1} \end{pmatrix} \tag{25}$$

2.2.2. Modeling of Line *L*

A line of length L can be represented by a quadrupole Q whose chain matrix is the following:

$$C_L = \begin{pmatrix} ch(\gamma L) & Z_M sh(\gamma L) \\ Y_M sh(\gamma L) & ch(\gamma L) \end{pmatrix} \tag{26}$$

With Z_M and Y_M are successively the impedance and the admittance of the free space.

2.2.3. Modeling of Unit *U*

The basic unit U_i consists of a discontinuity D_i and a line L_i (**Figure 3**), whose chain matrices C_D and C_L have already been determined.

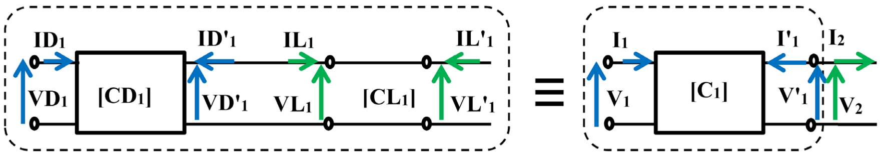

Figure 3. The equivalent circuit of a basic unit consisting of a discontinuity D and a line L.

From **Figure 3** and from the relation (25) we can write the relation that connects the parameters of the quadrupole CD_1:

$$\begin{pmatrix} VD_1 \\ ID_1 \end{pmatrix} = \begin{pmatrix} ZD_{11}ZD_{21}^{-1} & ZD_{12} - ZD_{11}ZD_{22}ZD_{21}^{-1} \\ ZD_{21}^{-1} & -ZD_{22}ZD_{21}^{-1} \end{pmatrix} \begin{pmatrix} VD_1' \\ ID_1' \end{pmatrix} \tag{27}$$

Similarly for the parameters of the quadrupole CL_1, we use relation (27); from where:

$$\begin{pmatrix} VL_1 \\ IL_1 \end{pmatrix} = \begin{pmatrix} ch(\gamma L_1) & Z_M sh(\gamma L_1) \\ Y_M sh(\gamma L_1) & ch(\gamma L_1) \end{pmatrix} \begin{pmatrix} VL_1' \\ IL_1' \end{pmatrix} \tag{28}$$

Figure 3 brings out the following equations:

$$ID_1 = I_1;\ VL_1' = V_1';\ IL_1' = I_1';\ VD_1' = VL_1;\ ID_1' = -IL_1$$

That we replace in relation (28) to becomes:

$$\begin{pmatrix} V_1 \\ I_1 \end{pmatrix} = \begin{pmatrix} ZD_{11}ZD_{21}^{-1} & ZD_{12} - ZD_{11}ZD_{22}ZD_{21}^{-1} \\ ZD_{21}^{-1} & -ZD_{22}ZD_{21}^{-1} \end{pmatrix} \begin{pmatrix} VL_1 \\ -IL_1 \end{pmatrix} \tag{29}$$

Then, we introduce the relation (28), the relation (29) becomes:

$$\begin{pmatrix} V_1 \\ I_1 \end{pmatrix} = CD_1 \cdot \begin{pmatrix} ch(\gamma l_1) & Z_M sh(\gamma l_1) \\ -Y_M sh(\gamma l_1) & -ch(\gamma l_1) \end{pmatrix} \begin{pmatrix} V_1' \\ I_1' \end{pmatrix} \tag{30}$$

If we write the input parameters of port N˚1 according to those of port N˚2, we will have the following relation:

$$\begin{pmatrix} V_1 \\ I_1 \end{pmatrix} = CD_1 \cdot CL_1 \begin{pmatrix} V_2 \\ I_2 \end{pmatrix} \tag{31}$$

with a passage chain matrix:

$$C_1 = CD_1 \cdot CL_1 \tag{32}$$

So, we can generalize (31) as following:

$$\begin{pmatrix} V_i \\ I_i \end{pmatrix} = C_i \begin{pmatrix} V_{i+1} \\ I_{i+1} \end{pmatrix} \tag{33}$$

2.2.4. Modeling of the General Chain *C*

The total chain consists of the concatenation of units U_i one after the other, and in the following we propose to determine the matrix of general passage relative to this chain. Indeed, a simple recurrence demonstration starting from the relation (33) can give the following generalization for all $n \geq 2$:

$$\begin{pmatrix} V_1 \\ I_1 \end{pmatrix} = \prod_{i=1}^{n-1} CD_i \cdot CL_i \begin{pmatrix} V_n \\ I_n \end{pmatrix} \tag{34}$$

We put the following form of the total chain matrix :

$$C = \prod_{i=1}^{n-1} CD_i \cdot CL_i \tag{35}$$

2.2.5. Modeling of Space Discontinuity *DS*

Referring to our previous work [4], we can write the unknown problem as:

$$X = M_{space}^{-1} A_1 I_n \tag{36}$$

and the input impedance of this discontinuity as:

$$Z_{DS} = A_1^t M_{space}^{-1} A_1 \tag{37}$$

2.2.6. Modeling of the Set

In summary, we first modeled the horn antenna as a sequence of discontinuities in a waveguide separated by a fixed distance (**Figure 1**), with the following formulation:

$$\begin{pmatrix} V_1 \\ I_1 \end{pmatrix} = C \begin{pmatrix} V_n \\ I_n \end{pmatrix} \tag{38}$$

Secondly, we have modeled the radiation of this horn in space by a discontinuity which opens on a charge representing the free space. Its formulation is as follows:

$$V_n = Z_{DS} I_n \tag{39}$$

We inject relation (39) into (38) one, we obtain the following system of equations:

$$\begin{cases} V_1 = C_{11} Z_{DS} I_n + C_{12} I_n & (40) \\ I_1 = C_{21} Z_{DS} I_n + C_{22} I_n & (41) \end{cases}$$

To determine the input impedance of the whole system, it suffices to divide V_1 by I_1:

$$Z_{in} = V_1 / I_1 = \left(C_{11} Z_{DS} + C_{12}\right) / \left(C_{21} Z_{DS} + C_{22}\right) \tag{42}$$

The self-reflection parameter S_{11} is then:

$$S_{11} = (z_{in} - 1)/(z_{in} + 1) \tag{43}$$

We determine I_n:

$$I_n = I_1/((C_{22} + C_{21})Z_{DS}) \tag{44}$$

And we return to relation (36) for the determination of the unknown problem:

$$X = M_{space}^{-1} A_1 \frac{1}{(C_{22} + C_{21})Z_{DS}} \tag{45}$$

3. Horn Array

In this part, we combine the modal analysis of Floquer with the methods used in the previous section to model a network of cornet waveguides.

3.1. Studied Structure

The present analysis considers an infinite periodic array of waveguides, from which a finite portion comprising nine horn antennas is extracted, as illustrated in Figure 4. Indeed, this arrangement allows us to study all types of coupling. The structure of element horn antenna is explained in Figure 5. These antennas are separated by a coupling distance d on the x-axis and on the y-axis. And they are radiate in a waveguide of dimension L_x, L_y and whose walls are periodic.

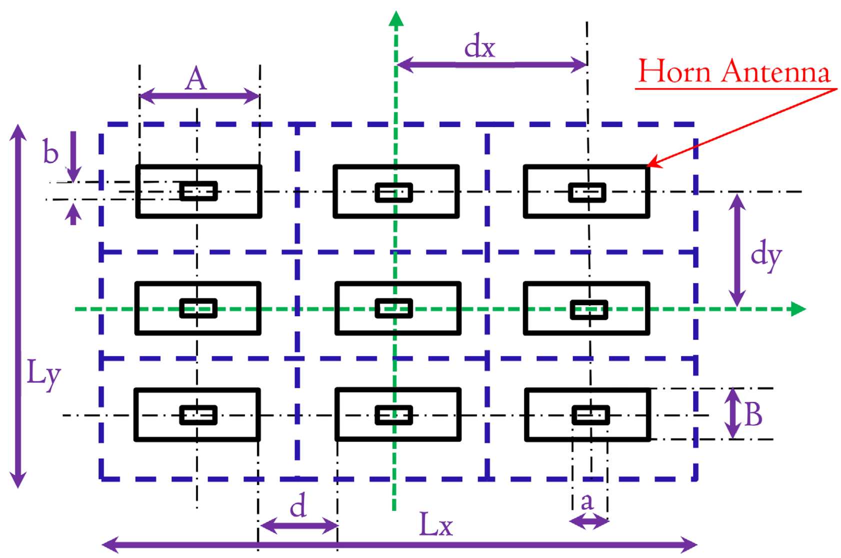

Figure 4. Representation of a subarray of nine horn waveguides.

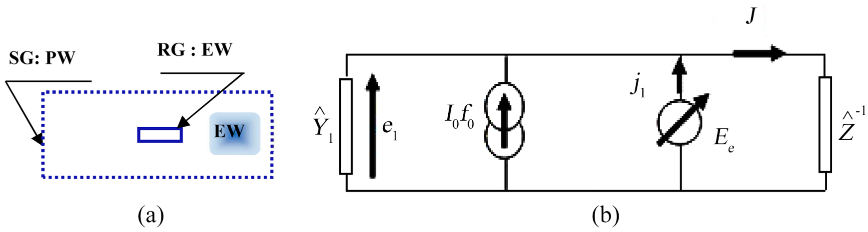

Figure 5. (a) An infinite rectangular waveguides array; (b) the relative equivalent circuit.

3.2. Problem Formulation

First, we consider the formulation of a rectangular waveguide presented in our previous work [Paragraph 2.2], and we change only the lateral walls of the space guide (SG) by periodic walls, as shown in **Figure 5**, to form an infinite rectangular waveguides array.

And we take the form of the unknown problem:

$$X = [y]^{-1} A I_0 \tag{46}$$

Second, we replace the excitation courant I_0 in (46) by I_n derived from (35) to build this time an infinite horn array.

Finally, we apply the Foquet modal analysis to this structure to constitute a finite horn array.

Indeed, the Floquet method permit to duplicate several times a unit cell on the x and y axes to form an array as desired. Then, the cell (i, s) is considered as a translation of the cell (0, 0) in space domain followed by another in the modal domain and expressed in dependence of the Floquet modes phases (α, β).

So, if we assume that:

- $(i, p) \in \mathbb{Z}^2$ and comprised within the range $\left[-\frac{N_x}{2}, \frac{N_x}{2} - 1\right]$.
- $(s, q) \in \mathbb{Z}^2$ and comprised within the range $\left[-\frac{N_y}{2}, \frac{N_y}{2} - 1\right]$.
- N_x and N_y are the numbers of array elements in the x and y directions respectively.
- L_x and L_y are the lengths of the array respectively according to the axes x and y.

α_p, β_q will have the following forms:

$$L_x = N_x d_x \tag{47}$$

$$L_y = N_y d_y \tag{48}$$

$$\alpha_p = \frac{2\pi p}{L_x} \tag{49}$$

$$\beta_q = \frac{2\pi q}{L_y} \tag{50}$$

So, the electric field at the position of cell (©, s) can be written as the superposition of the fields associated with the Floquet modes (spectral domain). And we can consider this decomposition as the transformation of the electric field of the space domain to modal domain. Mathematically this transformation is the inverse Fourier transforms (51).

Similarly, the field that radiates a phase shift cell can be written as a sum of the radiated energy of this field on all cells. This summation can be seen as the Fourier transform of the electric field of the modal domain in space domain (52).

$$E(i, s) = \frac{1}{\sqrt{N_x N_y}} \sum_{p,q} \tilde{E}_{\alpha_p, \beta_q} \mathrm{e}^{j\alpha_p (idx)} \cdot \mathrm{e}^{j\beta_q (sdy)} \tag{51}$$

$$\tilde{E}_{\alpha_p,\beta_q} = \frac{1}{\sqrt{N_x N_y}} \sum\nolimits_{i,s} E\left(id_x, sd_y\right) \cdot \mathrm{e}^{-j\alpha_p(id_x)} \cdot \mathrm{e}^{-j\beta_q(sd_y)} \tag{52}$$

It has been demonstrated [4] [5] that these transformations lead to expressions emphasizing the coupling terms established between array elements such as the Z, Y and S parameters, we present here Z matrix:

$$\left[Z_{i,s}\right] = TF^{-1}\left[\tilde{Z}_{\alpha_p,\beta_q}\right]TF \tag{53}$$

with, $\left[\tilde{Z}_{\alpha_p,\beta_q}\right]$ is a spectral representation of the diagonal matrix that concatenates the intrinsic input impedance associated with a cell Floquet modes of the array.

4. Numerical Results

4.1. Horn Waveguide

In this section we propose to study the distribution of the electric field, at the plane of discontinuity, and on the radiation pattern of a horn antenna as a function of its shape of the profile. To do this, a reference horn antenna shown in **Figure 6** was chosen. We have kept the dimensions a, b and rh invariable, and we have varied the dimensions A and B which are called D. The dimensions of the reference antenna are named ***Dref*** and presented in **Figure 6**.

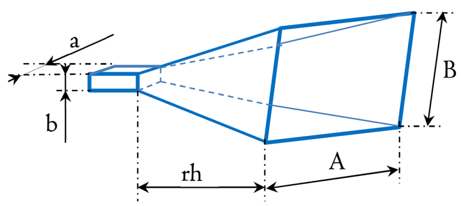

$a = 22.86$ mm

$b = 10.16$ mm

$rh = 131.06$ mm

$A = 67.31$ mm

$B = 49.37$mm

Figure 6. The reference horn antenna with $re = rh$.

In **Figure 7**, we determine the distribution of the electric field at the aperture of the reference horn guide.

To study the influence of the shape of profile on this distribution we consider three cases. And we trace in the same **Figure 8** a central section of each field. We are therefore interested in the shape of the electric field without taking into account the actual dimensions of the surface of discontinuity. Indeed, we have subdivided each time the surface of discontinuity by one hundred.

Figure 8 shows that the more we enlarge the aperture more the distribution of the field at these aperture concentrates in the middle.

The radiation patterns of the three aforesaid horn antennas are shown in **Figure 9**. Again, we note that when the antenna apertures widen, the amplitudes of the secondary lobes diminish.

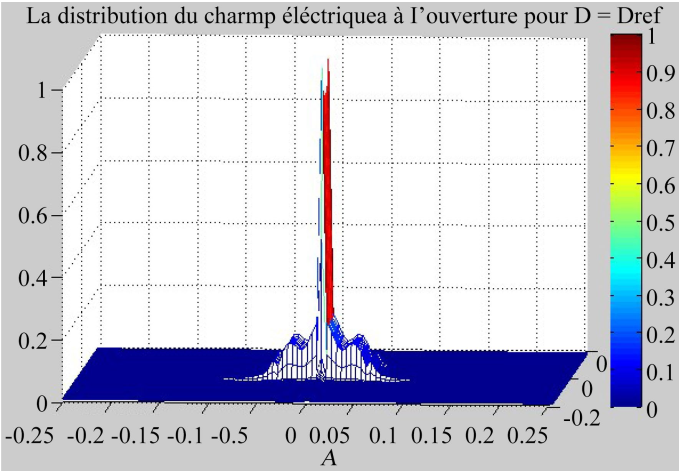

Figure 7. The normalized distribution of the electric field to the plane of discontinuity of a reference horn antenna.

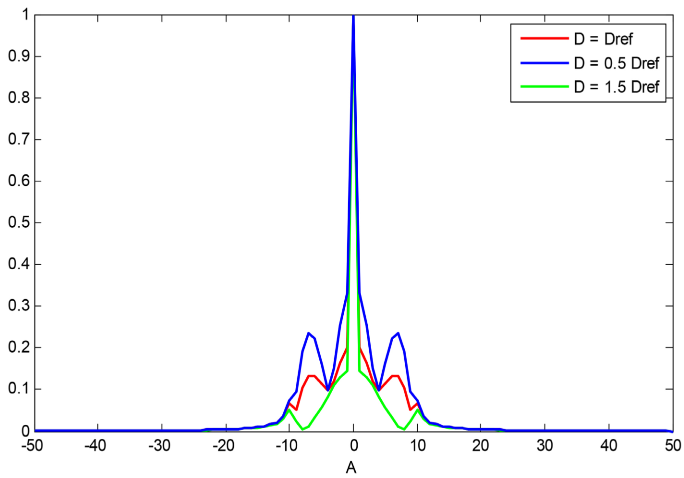

Figure 8. The comparison of the normalized distribution of the electric field in the discontinuity plane for the three cases: $D = Dref$, $D = 0.5Dref$ and $D = 1.5Dref$.

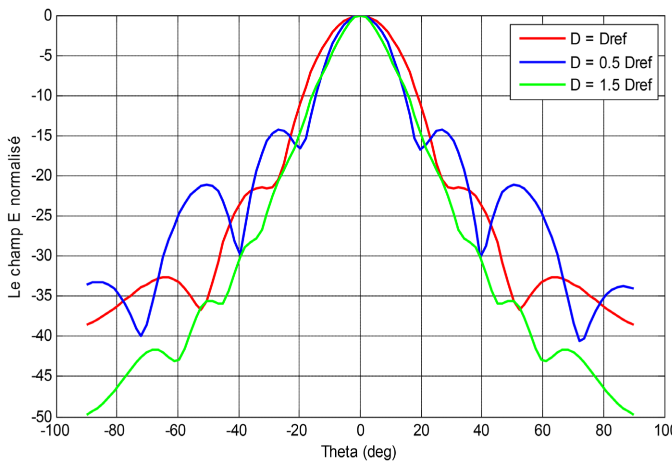

Figure 9. The comparison of the radiation patterns of the cornet guides in the three cases: $D = Dref$, $D = 0.5Dref$ and $D = 1.5Dref$.

This study shows that the dimensions of the reference antenna present a judicious choice, which answers the compromise more directivity and less congestion.

4.2. Horn Array

In this section we study the horn array antenna through the parameters S and the distribution of the electric field at the discontinuity plane as a function of the coupling distance d. And we considered the same cases of study: (a) $d_1 = 2\lambda$; (b) $d_2 = \lambda$; (c) $d_3 = 0.1\lambda$.

4.2.1. Scattering Parameters

When we determine the S parameters matrix for the different coupling distances, we remark that there are values that are repeated, and their positions in matrix do not change regardless of the coupling distance. So, we determine nine sets composed by nine parameters that have a same value each one. In Table 1, we consider the center cell and we present the mutual coupling coefficient, interacting with it, as a function of the coupling distance d. All other parameters have same values. These physical magnitudes present the percentages of powers relating to these parameters with respect to the power initially issued.

Table 1. Horn array scattering parameters as functions of coupling distance ***d***.

$d\,(\lambda)$	$\lvert S_{55}\rvert^2$	$\lvert S_{45}\rvert^2$	$\lvert S_{65}\rvert^2$	$\lvert S_{25}\rvert^2$	$\lvert S_{85}\rvert^2$	$\lvert S_{75}\rvert^2$	$\lvert S_{35}\rvert^2$	$\lvert S_{95}\rvert^2$	$\lvert S_{15}\rvert^2$
2	0.0348	0.0055	0.0057	0.0126	0.0036	0.0002	0.0010	0.0002	0.0027
1	0.0478	0.0201	0.0175	0.0388	0.0056	0.0034	0.0019	0.0034	0.0285
0.1	0.0737	0.0459	0.0372	0.0785	0.0278	0.0057	0.0029	0.0057	0.0340

To understand the physical meaning of these parameters we define three follow types of power:

- Self-reflected Power: $SP = S_{ii}^2$
- Coupling Power: $CP = \sum_{i \neq j} S_{ij}^2$
- Radiated power: $RP = 1 - (SP + CP)$

And we present these powers in Table 2.

Table 2. Three powers as functions of coupling distance ***d***.

d en (λ)	PA	PC	PR
2	0.0348	0.0336	0.9315
1	0.0478	0.1256	0.8266
0.1	0.0737	0.2551	0.6712

We can notice that the self-reflective powers and coupled powers are inversely proportional to the coupling distance d, rather radiated powers which are proportional to the distance.

4.2.2. Electric Field Distribution

The electrical field distributions in **Figure 10** show that the coupling varies inversely proportionally to the coupling distance and the boundary conditions are respected even for a coupling distance of the 0.1λ order.

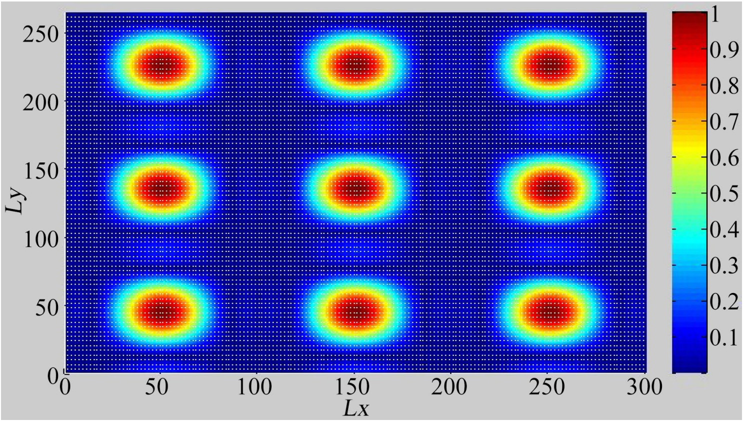

(a) La distribution normaliséee du champ Ed = 2Lambda

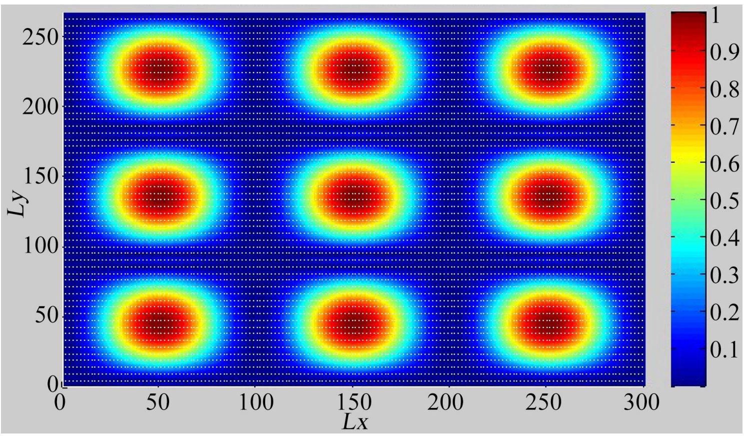

(b) La distribution normaliseee du champ Ed = Lambda

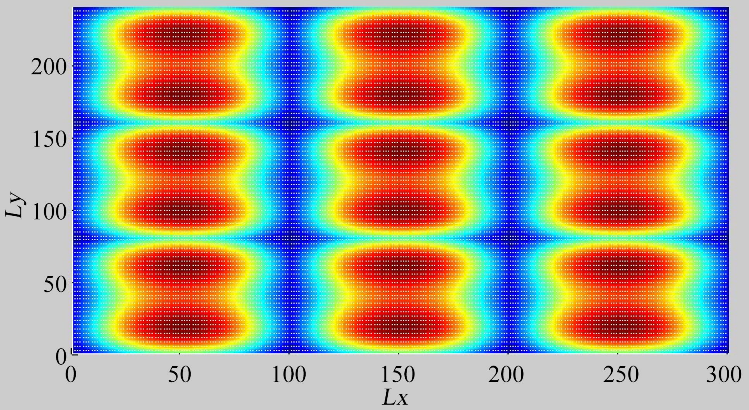

(c) La distribution normaliseee du champ Ed = 0.1Lambda

Figure 10. The normalized distribution of the electric field to the discontinuity surface for a network of nine cornet waveguides with a coupling distance: (a) $d_1 = 2\lambda$, (b) $d_2 = \lambda$, et (c) $d_3 = 0.1\lambda$.

5. Conclusions

This paper has presented a rigorous and systematic two-step formulation for the analysis and optimization of a horn antenna array. The approach first focused on optimizing a single pyramidal horn element in a standalone configuration before extending the analysis to the array environment.

For the isolated horn, a parametric study of the aperture and flare dimensions demonstrated a direct and significant influence on the antenna's directivity. The results confirm that directivity increases with the physical dimensions of the horn aperture. However, this relationship is subject to diminishing returns; beyond a certain threshold, the marginal gain in directivity no longer justifies the corresponding increase in size, weight, and material cost. This initial study was therefore crucial for determining an optimal horn geometry that balances radiative performance with practical constraints.

In the array configuration, the synthesis via Floquet modal analysis revealed that the overall performance of the antenna system can be further optimized by adjusting the inter-element spacing. Specifically, it is shown that reducing the distance between adjacent horn elements allows for a more compact array footprint while maintaining favorable radiation characteristics, thereby optimizing the system's spatial efficiency.

In summary, the proposed hybrid MoM-GEC and Floquet-based methodology provides an effective and computationally efficient framework for the design of high-performance horn arrays, enabling concurrent optimization of both the individual element geometry and the array lattice.

Conflicts of Interest

The authors declare no conflicts of interest regarding the publication of this paper.

References

[1] Ram, G., Mandal, D., Kar, R. and Ghoshal, S.P. (2013) Optimized Hyper Beamforming of Linear Antenna Arrays Using Collective Animal Behaviour. *The Scientific World Journal*, **2013**, Article ID: 982017. https://doi.org/10.1155/2013/982017

[2] Ghatak, K., Senapati, A. and Sekhar Roy, J. (2015) Investigations on Adaptive Beamforming for Linear and Planar Smart Antenna Arrays Using Sample Matrix Inversion Algorithm. *International Journal of Computer Applications*, **117**, 47-50. https://doi.org/10.5120/20578-2987

[3] Kaddouri, A., Aidi, M. and Aguili, T. (2016) A New Formulation of Open Ended Waveguide Radiating in Free Space Based on MoM-GEC Method. *International Journal of Microwave & Optical Technology*, **11**, 115-122.

[4] Kaddouri, A., Aidi, M. and Aguili, T. (2015) A New Approach Based on MoM-GEC Method to Mutual Coupling Analysis of Symmetric Twin Waveguides for Antenna Applications. *Journal of Electromagnetic Analysis and Applications*, **7**, 283-290. https://doi.org/10.4236/jemaa.2015.712030

[5] Kaddouri, A., Hamdi, B., Aidi, M. and Aguili, T. (2018) Global Method Combined with Floquet Modal Analysis to Model an Antenna Based on Rectangular Waveguide Array. *EPH—International Journal of Science and Engineering*, **4**, 47-55.

https://doi.org/10.53555/eijse.v4i2.171

[6] Hotte, D., Siragusa, R., Duroc, Y. and Tedjini, S. (2015) Directive and High-Efficiency Slotted Waveguide Antenna Array for V-Band Made by Wire Electrical Discharge Machining. *Electronics Letters*, **51**, 380-382. https://doi.org/10.1049/el.2014.4409

[7] Bird, T.S. and Granet, C. (2007) Optimization of Profiles of Rectangular Horns for High Efficiency. *IEEE Transactions on Antennas and Propagation*, **55**, 2480-2488. https://doi.org/10.1109/tap.2007.904114

[8] Yeap, K.H., Wong, E.V.S., Nisar, H., Lai, K.C. and Ng, C.A. (2017) Attenuation in Circular and Rectangular Waveguides. *Electromagnetics*, **37**, 171-184. https://doi.org/10.1080/02726343.2017.1301198